Nevada Bureau of Mines and Geology Open-File Report 2023-13

RECONNAISSANCE GEOLOGIC AND GEOMORPHIC EVALUATION OF THE 2023 LANDSLIDE ALONG THE SOUTHERN FLANK OF PEAVINE MOUNTAIN, RENO, NEVADA

Rich D. Koehler, James E. Faulds, and Aren T. Crandall-Bear
Nevada Bureau of Mines and Geology, University of Nevada, Reno

2023

Nevada Bureau of Mines and Geology
nbmg.unr.edu

University of Nevada, Reno

Suggested citation:
Koehler, R.D., Faulds, J.E., and Crandall-Bear, A.T., 2023, Reconnaissance geologic and geomorphic evaluation of the 2023 landslide along the southern flank of Peavine Mountain, Reno, Nevada: Nevada Bureau of Mines and Geology Open-File Report 2023-13, 16 p.

© Copyright 2023 The University of Nevada, Reno.
All Rights Reserved.

ABSTRACT

In the spring of 2023, a landslide occurred on the south flank of Peavine Mountain west of Reno, Nevada near the residential community of Somersett and in the vicinity of future planned developments. The Nevada Bureau of Mines and Geology conducted an investigation to document the site characteristics, assess possible factors that may have contributed to the failure, and determine when the slide occurred. Analysis of InSAR data indicates that the landslide occurred between April 26 and May 1, 2023. The field observations indicate that the slide was a bedrock translational block slide/slump associated with extension along the head scarp and buckling at the toe of the slide. The dominant contributing factors include saturation of the subsurface related to above normal precipitation during the 2022/2023 winter, record high temperatures on April 28–29 leading to accelerated snow melt, and clay weathering of the bedrock and associated discontinuities. It is recommended that future developments in the area implement focused geotechnical studies to assess additional landslide hazards.

INTRODUCTION

This report presents the findings of a reconnaissance geologic and geomorphic evaluation conducted by the Nevada Bureau of Mines and Geology (NBMG) of a landslide that occurred along the south flank of Peavine Mountain west of Reno, Nevada in the spring of 2023. The landslide occurred along an unnamed stream channel within the Verdi 1:24,000-scale topographic quadrangle northwest of the Somersett residential development (figure 1). Although the upper slopes of Peavine Mountain in the area of the landslide are undeveloped, areas along the base of the mountain have experienced rapid development, including 1) residential projects associated with the communities of Somersett, Del Webb, Mogul, and Verdi, 2) industrial warehousing and storage facilities, and 3) U.S. Interstate 80, a vital transportation corridor.

From October 2022 to May 2023, the Reno area experienced excessive rain and snowfall with the occurrence of over 10 atmospheric rivers, resulting in greater than 13.72 inches of precipitation, nearly 200% of the average annual precipitation (NOAA, 2023). The landslide occurred within steep terrain at an elevation of 1695 m (5560 ft) approximately 820 m (2,690 ft) northwest of the Somersett development and 535 m (1755 ft) west of a four-wheel drive dirt road, locally known as Hawk Meadow Trail (GPS coordinates 39.545208, -119.960529) (figures 1 and 2). The landslide was originally reported to NBMG on May 27, 2023 by a concerned citizen who noted a "crack in the earth". Although the exact timing of the landslide is unknown, one of the authors was hiking in the area on April 9 and was turned back by deep snow at ~6,000 ft (1,829 m) elevation. The landslide was not observed on that date, as substantiated by photographic evidence. However, substantial snow cover above ~6,000 ft and saturated soils throughout the area were observed on April 9, both of which may have contributed to subsequent slope failure in mid-April to late May, 2023.

Given the occurrence of the 2023 landslide, this reconnaissance study was motivated by the existence of recent developments directly to the southeast of the slide feature, proposed developments downstream and within the site vicinity, and the possibility of future potentially damaging landslides. The main purpose of this investigation was to document the characteristics of the 2023 surface movement and assess the local geomorphic, bedrock, and climatic conditions that may have contributed toward the failure. Field reconnaissance of the landslide and site vicinity was conducted by NBMG geologists on June 4 and 6, 2023 and August 23, 2023. The scope of the investigation included review of previous geological mapping, inspection of National Agricultural Imagery Program (NAIP) images and lidar hillshade data (Digital Aerial Solutions, 2018), assessment of slope topography, photo documentation of the landslide, measurements of associated cracks and escarpments, and description of exposed colluvial materials. Additionally, an analysis of InSAR data was conducted to further constrain the timing of the landslide and test whether deformation could be observed from satellite data.

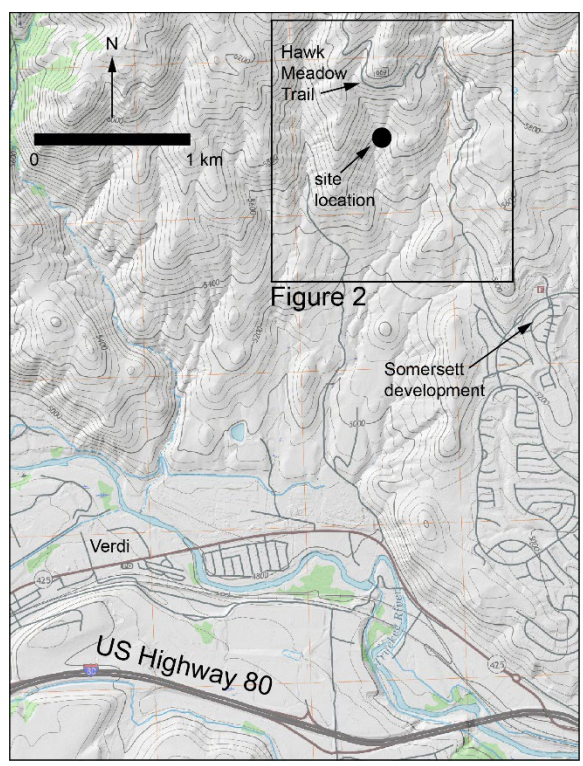

Figure 1. Location of the landslide (black circle) plotted on the 7.5'-scale Verdi topographic quadrangle. Location of figure 2 shown by black box.

GEOMORPHIC AND GEOLOGIC CONDITIONS OF THE LANDSLIDE SITE VICINITY

The site vicinity is characterized by relatively steep south-facing slopes with north-south-trending ridges and stream valleys. Upslope of the landslide, slopes are locally greater than 19° (35%) and characterized by exposed bedrock and thin colluvial cover. Ephemeral stream channels are typically eroded into bedrock within upper slope areas and grade downslope to narrow channels filled with slope colluvium that is in places greater than 2 m thick. Lower slope areas are characterized by relatively gentle bedrock slopes 6° (12%) and alluvial-fan surfaces 3° (6%) that grade to relatively flat fluvial terrace surfaces of the Truckee River. Alluvial-fan surfaces range in age from middle Pleistocene to Holocene and range in thickness from a few meters to over 10 m (Faulds et al., in review).

Inspection of NAIP imagery and lidar hillshades indicates the presence of steep narrow gorges, broad arcuate hollows, and cuspate swales suggesting that prior landsliding and debris flows have sculpted the topography in the past (figures 2 and 3). Although few landslide deposits have been identified along the southern slope of Peavine Mountain (Faulds et al, in review), bedrock benches present in some stream valleys beneath cuspate slope hollows may be the geomorphic expression of prior landsliding. Based on the presence of alluvial fans in downslope areas, debris flows that scour stream channels and transport sediment to the lower slopes are the most common type of mass wasting process in the area.

The local slopes across the 2023 landslide prior to its occurrence are shown on the maps in figure 3, and topographic profiles are illustrated in figure 4. Directly above the head scarp, the terrain is relatively steep and slopes 20° (39%), whereas the slope across the center of the slide mass is relatively gentle around 8° (14%). The slope steepens across the toe of the slide mass to 24° (45%) within the stream channel.

Bedrock underlying the landslide site consists of Miocene porphyritic andesite lavas of Peavine Mountain that dip moderately (~25–65°) southeast and are cut by northerly to northeast-striking normal faults (figure 2C) (Faulds et al., in review). These rocks are medium to dark

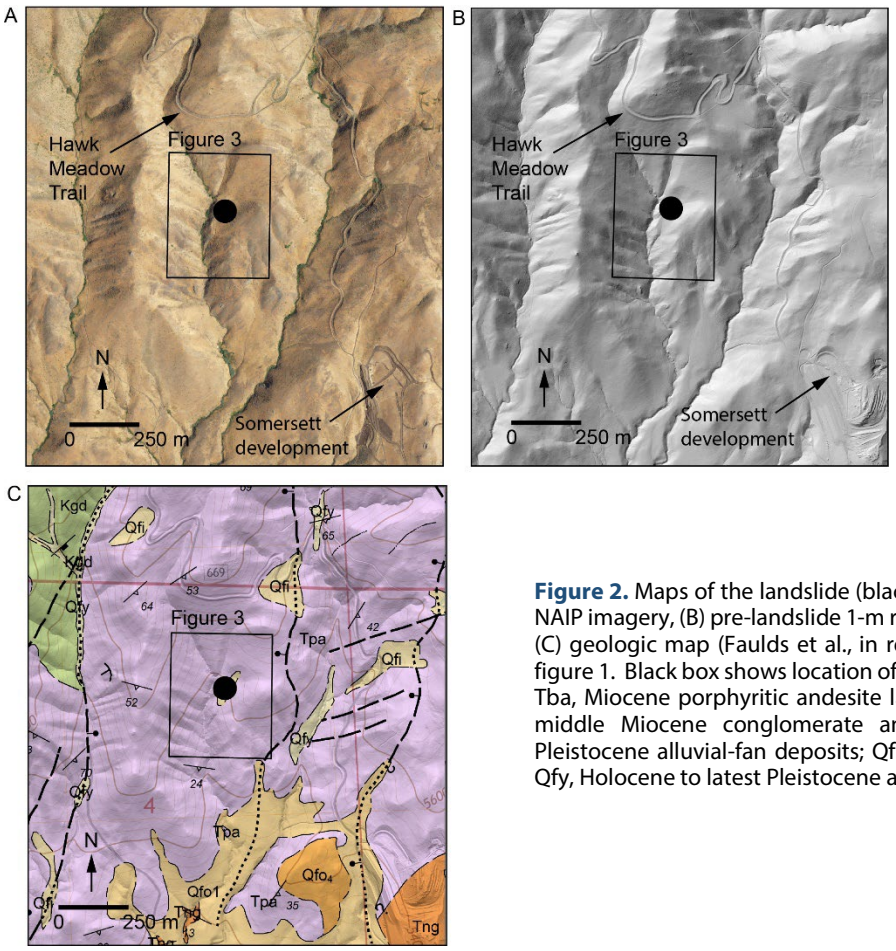

Figure 2. Maps of the landslide (black circle) site vicinity including (A) 2017 NAIP imagery, (B) pre-landslide 1-m resolution lidar bare earth hillshade, and (C) geologic map (Faulds et al., in review). Area of this figure is shown on figure 1. Black box shows location of figure 3. Kgd, Cretaceous granodiorite; Tba, Miocene porphyritic andesite lavas of Peavine Mountain; Tng, late to middle Miocene conglomerate and sandstone; Qfo1, late to middle Pleistocene alluvial-fan deposits; Qfi, late Pleistocene alluvial-fan deposits; Qfy, Holocene to latest Pleistocene alluvial-fan deposits.

gray, relatively massive lavas and flow breccias with minor interbedded conglomerate. Compositions range from andesite to basaltic andesite and are most commonly finely porphyritic lava with phenocrysts of plagioclase (30–40%, 1–2 mm), clinopyroxene (5–10%, 1–3 mm), and hornblende (0–5%, 1–4 mm). Altered and weathered rocks are scattered through the area and are generally reddish to yellowish brown with feldspars generally altered to clays, and mafic minerals (hornblende) altered to iron oxides.

These weathering products contribute toward the development of clay-rich colluvial soils. The andesite lavas nonconformably overlie late Cretaceous granite to the north and are overlain to the south by late Miocene sedimentary rocks, including conglomerate, sandstone, and diatomaceous shale.

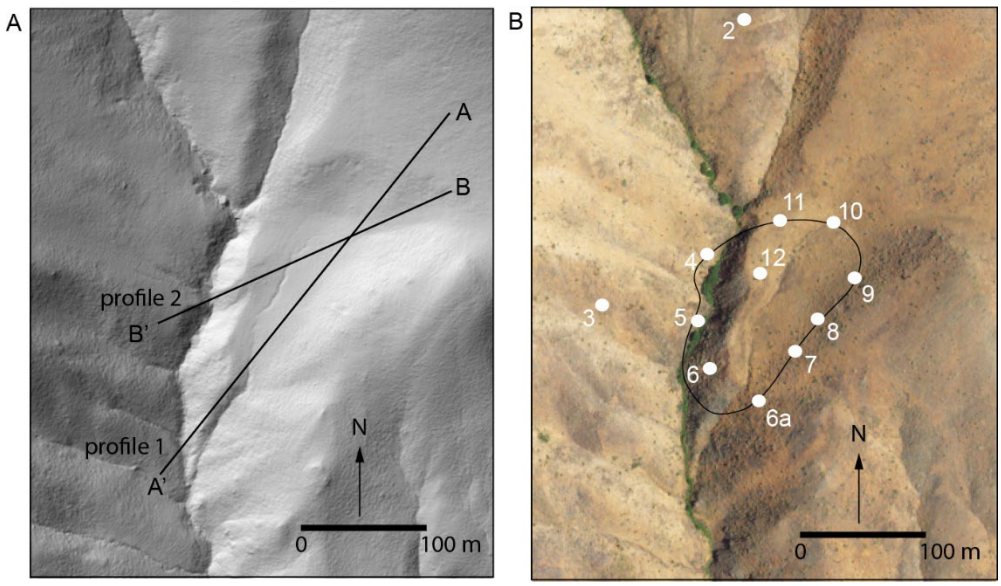

Figure 3. Fine-scale images of the slide feature including (A) pre-landslide bare earth lidar hillshade, and (B) 2017 NAIP imagery showing observations points (numbered white circles) and extent of slide mass (thin black line). Numbered observation points correlate to those listed in table 1. Observation point number 1 is along the access road north of the slide and not included here.

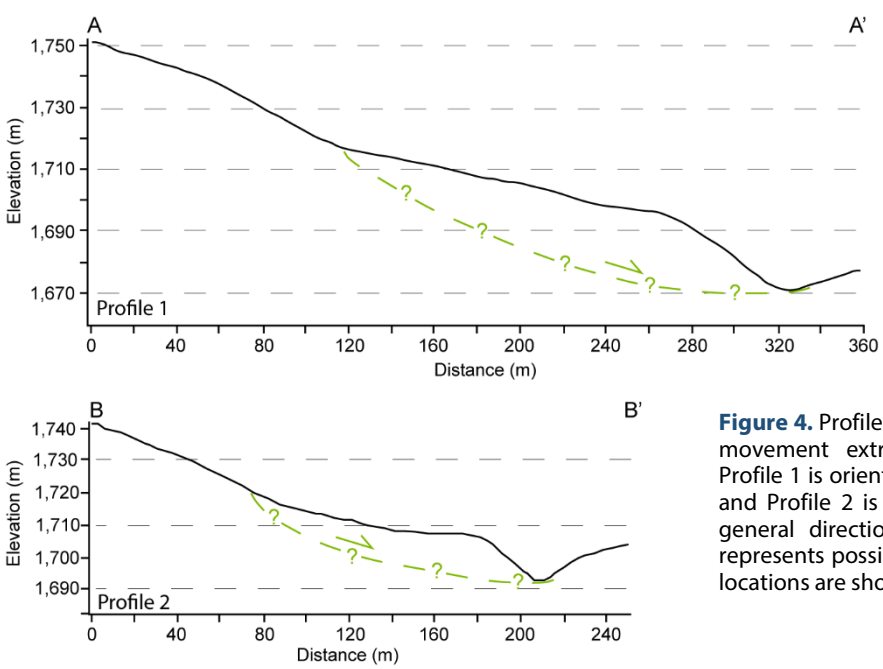

Figure 4. Profiles 1 and 2 of the ground surface prior to movement extracted from lidar topographic data. Profile 1 is oriented in a generally downslope direction, and Profile 2 is oriented across the slide mass in the general direction of movement. Dashed green line represents possible geometry of the slide plane. Profile locations are shown on figure 3.

RECONNAISSANCE OBSERVATIONS

Photographs of the landslide during the June and August reconnaissance are shown on figures 5 and 6. The green vegetation in the June photographs reflects the wet soil conditions in the spring, and the brown to yellow vegetation in the August photographs reflects the more typical dry conditions in the late summer. The location of individual field observations (site numbers) are shown on figure 3B, and a summary of the observations is provided in table 1. Field photographs from the observation sites are provided in appendix A.

The main head scarp is arcuate in shape, generally faces west, and is associated with normal slip of the ground surface along the head scarp and within a series of small extensional grabens (sites 6a–11). Dip-slip striae were observed along the head scarp in early June 2023 along slip surfaces dipping about 60 to 80° south and west. Vertical separation of the ground surface across the head scarp ranges from 50–90 cm. The free face below the crown of the landslide exposes colluvium and ranges in height between 90 cm and 2.5 m. Extensional grabens along the head scarp range in width between 1 and 3.5 m and are typically bound by open cracks up to 1.5 m deep. A zone of transverse cracks (extensional openings orthogonal to the direction of flow) up to 1.5 m deep and 20–40 cm wide extends across the slide approximately 15 m to the west of the head scarp (site 9). All of the features within and adjacent to the head scarp are consistent with motion down to the south and west of the upper part of the landslide.

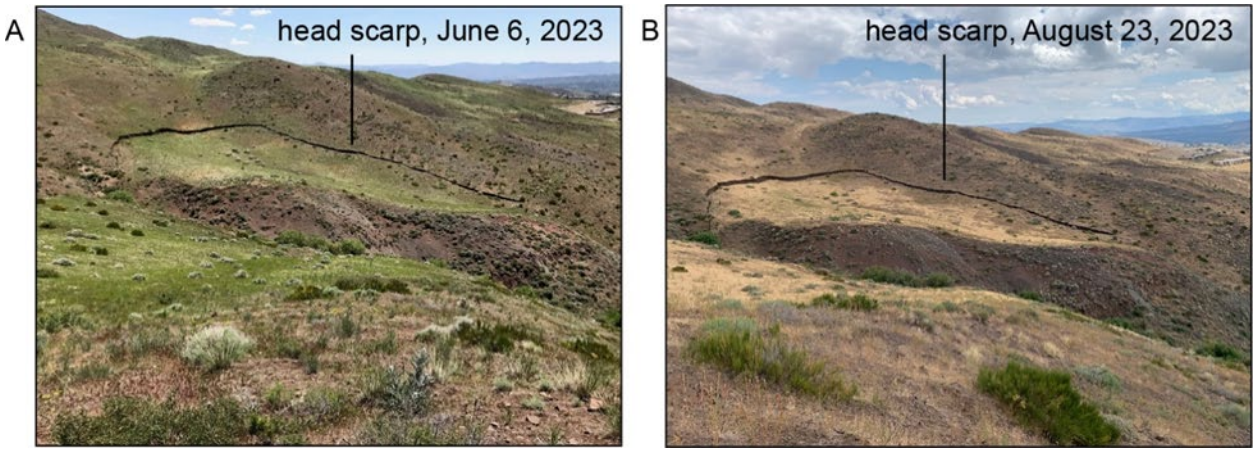

Figure 5. Photographs of the head scarp and slide mass showing site conditions in June, 2023 (A) and August, 2023 (B), indicating that the slide has experienced little movement since it occurred. View to the east from similar vantage point in each photo.

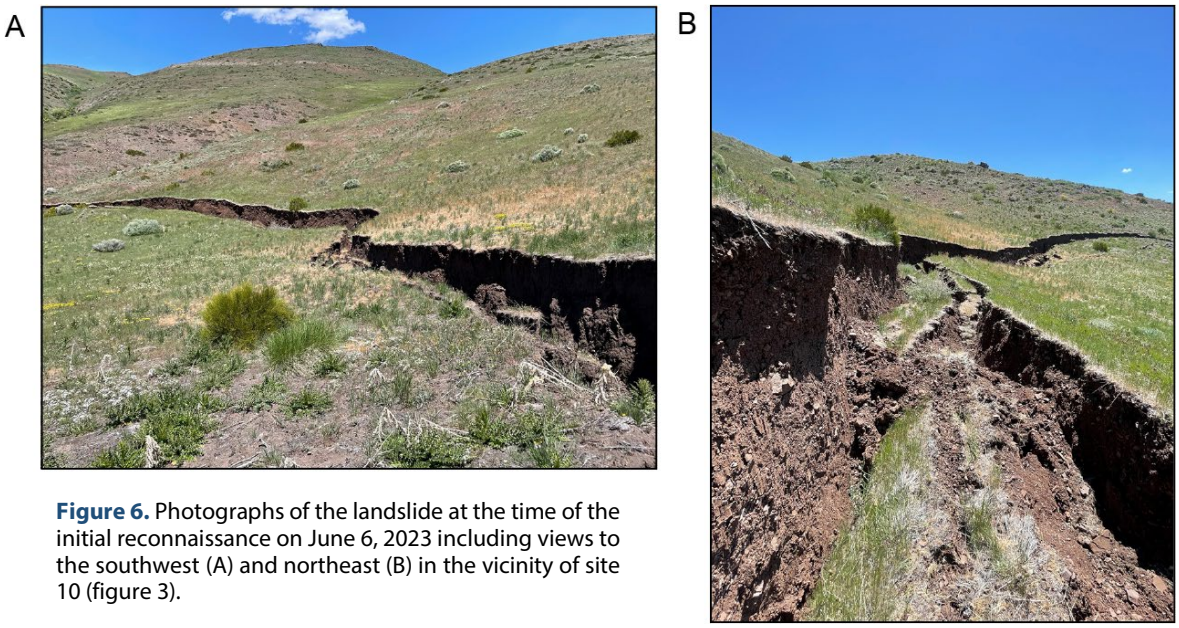

Figure 6. Photographs of the landslide at the time of the initial reconnaissance on June 6, 2023 including views to the southwest (A) and northeast (B) in the vicinity of site 10 (figure 3).

The toe of the landslide is characterized by two approximately 30-m-long thrust scarps up to 1.5 m in height (sites 4 and 5). Both scarp faces show slickenlines within the clay-rich colluvium that plunge 46° N, consistent with up-to-the-west and south-motion of the slide toe. This transport direction is also consistent with radial cracks within the central part of the slide mass (site 12). The presence of the thrust scarps suggests that the slide plane may extend beneath the base of the stream channel.

Colluvial sediments exposed in the head scarp and along the toe of the landslide consist of clayey sand to sandy clay loam with carbonate nodules and <10% subangular gravels and cobbles up to 10 cm in diameter sourced from the local bedrock. The colluvial sediments are relatively thick (>2 m) in the upper part of the slide mass and thin to <20 cm along the eastern stream channel margin near the toe of the landslide, where weathered bedrock is locally exposed. At site 6, a zone of subparallel extensional cracks (up to 60 cm wide and 1.4 m deep) and transverse ridges (thrusts of soil orthogonal to the direction of flow) bend around the toe of the landslide and project toward the head scarp at site 6a.

Table 1. GPS locations and summary observations from sites visited during the August 23, 2023 reconnaissance. Observation site locations shown on figure 3 and photographs from each site are contained in appendix A.

Site #	Latitude	Longitude	Observations
2	39.547093	-119.960904	Vantage point from north of the landslide. Landslide is along east flank of unnamed stream valley. Slide mass along the lower part of the slope.
3	39.545081	-119.962199	Vantage point from west of the landslide. Arcuate shaped head scarp. Slide mass transport direction toward west bank of unnamed stream channel and slightly south.
4	39.545446	-119.961249	Uphill-facing scarps along the lower western stream bank. Scarps expose colluvial sediment consisting of clayey sand to sandy clay loam with trace subangular gravels and cobbles. Scarp is 30 m long and up to 80 cm high. Clay slickenlines indicate thrusting to the west-southwest along the toe of the slide.
5	39.544976	-119.961324	Uphill-facing scarp along the lower western stream bank. Scarp exposes clayey sand colluvium with carbonate nodules and <10% subangular gravel and cobbles up to 4 cm diameter. Scarp is about 31 m long and up to 1.5-m-high. Clay slickenlines plunge 46° north and indicate south directed thrusting of the slide toe.
6	39.544639	-119.961221	Subparallel extensional cracks and transverse ridges in the east wall of stream channel. Cracks are up to 60 cm wide and 1.4 m deep. Cracks generally oriented south-southeast and bend to more easterly orientation around the toe of the slide, projecting toward the head scarp (site 6a). Weathered bedrock and thin colluvium exposed in the slope. Talus cones consisting of angular cobbles indicate rockfall during sliding.
6a	39.54415	-119.960780	Southern end of landslide head scarp associated with 1.7-m-high free face and open crack 1.1 m wide. Head scarp exposes colluvial sediments.
7	39.544767	-119.960452	Head scarp along southeastern margin of landslide with 1.5-m-high free face associated with an extensional graben 1.7 m wide. Vertical separation of the ground surface about 50 cm. Head scarp exposes colluvial sediments.
8	39.544989	-119.960244	Head scarp along southeast margin of landslide with 2.5-m-high free face associated with extensional graben 1.4 m wide. Vertical separation of ground surface about 90 cm. Head scarp exposes colluvial sediments.
9	39.545280	-119.959904	Easternmost part of landslide head scarp with 2.8-m-high free face associated with extensional graben 2.4 m wide. Vertical separation of ground surface about 70 cm. Head scarp exposes colluvial sediments. Zone of multiple transverse cracks up to 1.5 m deep extend across the slide approximately 15 m to the west of the head scarp.
10	39.545662	-119.960110	Head scarp along the northern margin of the landslide with 2.4-m-high free face associated with extensional graben 3.5 m wide. Vertical separation of the ground surface about 70 cm. Head scarp exposes colluvial sediments.
11	39.545683	-119.960589	Head scarp along the northwestern margin of the landslide with 90-cm-high free face associated with extensional graben 3 m wide. South side of graben bound by fissure 90 cm deep and 20 cm wide. Vertical separation of ground surface about 50 cm. Total extension across graben around 80 cm.
12	39.545310	-119.960766	Multiple subparallel cracks (radial cracks) in the west-central part of the slide mass. Individual cracks up to 50 cm deep and 25 cm wide. Indicates a component of slide mass motion to the south toward the major drainage channel.

*Site #1 is along the access road north of the slide and not included here.

InSAR ANALYSIS

The Interferometric Synthetic Aperture Radar (InSAR) data coverage for the area consists of data from the European Space Agency Sentinel mission. Two ascending and two descending look directions covered the area of the landslide, for a total of four tracks. Given the initial constraints on the timing of the slide from field observations (mid-April to May 27, 2023), epoch dates of InSAR scenes were chosen to cover the time window between early April and mid-June, 2023, to create a short time series. Epoch dates were selected to be the same for ascending and descending tracks, giving no additional constraint on the timing of the slide between ascending and descending look directions.

Interferograms were processed using the InSAR for Scientific Computing Environment (ISCE) software package from the Jet Propulsion Laboratory, with multi looking set to 1 azimuth look and 6 range looks, resulting in a pixel size of ~14.0 m range by 15.6 m azimuth. Enhanced Spectral Diversity (ESD) correction did not result in any noticeable change in the signal. The time series was generated with the Miami INsar Time-series software in Python (MintPy). InSAR images were generated from differencing between epochs in the time series and were de-ramped to remove long wavelength errors in the images resulting from, for example, moisture in the troposphere. The time series of nearby pixels and pixels of interest were median filtered. InSAR map views and time-series plots are shown in figures 7 and 8.

The interferograms likely have unwrapping errors in the area around the slide due to its small size (~50 by 20 m, as recognizable in the InSAR data) compared to the size of the InSAR pixels, resulting in the absence of fringes as would be seen in an earthquake that would cause a similar amount of deformation over a larger area. The small size of the signal leads to a potential for unwrapping errors. Due to likely unwrapping errors, any deformation seen in the InSAR images and time series are uncertain by an integer n multiplied by 2π and the SAR wavelength (~5.55 cm). The observed deformation within the slide mass (positive line of sight deformation up to 10 mm) is much less than the displacements observed in the field (up to 3 m lateral and

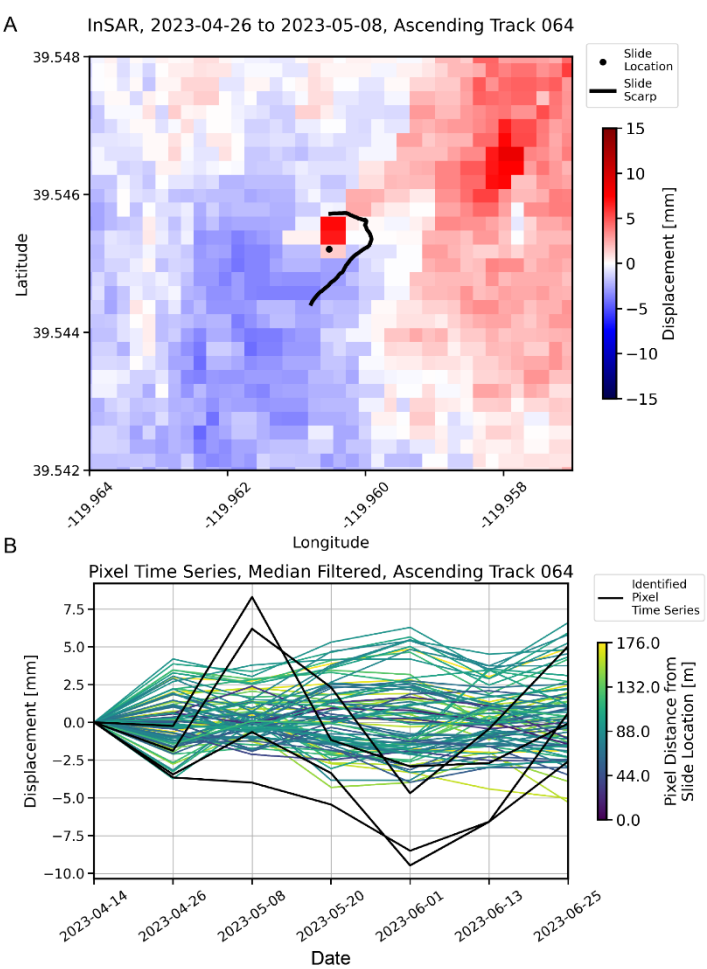

Figure 7. (A) InSAR map view of time series result between epochs of 04-26 to 05-08, 2023. Identified pixels are within the slide mass and stand out from surrounding pixels with regards to displacement (red pixels within the slide mass). InSAR image has been de-ramped. (B) Time series plot of identified pixels (black) and nearby pixels colored by distance from center of the slide. Identified pixels are selected from figure 7A. The time series of these pixels (black, and correspond to the red pixels within the slide mass in figure 7A) stand out compared to nearby pixels. Time series has been median filtered. Movement beyond median filtered neighbor time series is seen between 04-26 and 05-08, 2023.

vertical). This is likely due to the inability of standard algorithms to fix unwrapping errors described above, because there are only a few pixels covering the slide, so the n number of 2π steps in the interferometric phase cannot be clearly identified. Hence, InSAR results should not be taken to indicate that the displacement was only ~1 cm but can be used to constrain timing and spatial extent of the slide.

The timing of the slide can be constrained from the de-ramped InSAR images by comparing median filtered time series of effected pixels to surrounding pixels. A signal can be seen in the two ascending look directions (figures 7 and 8). However, no signal is seen in either of the descending look directions. The absence of a signal in the descending look directions could be caused by unwrapping errors, or a poor line of sight, as the topography is angled away from the descending look direction in the area of the slide. The dates of ascending and descending epochs are the same, and thus no additional timing constraint is lost from having no observable signal in the descending look direction. The results indicate that the slide occurred between April 26, 2023 and May 1, 2023, with some additional movement occurring in the following weeks, possibly owing to continued slip or settlement.

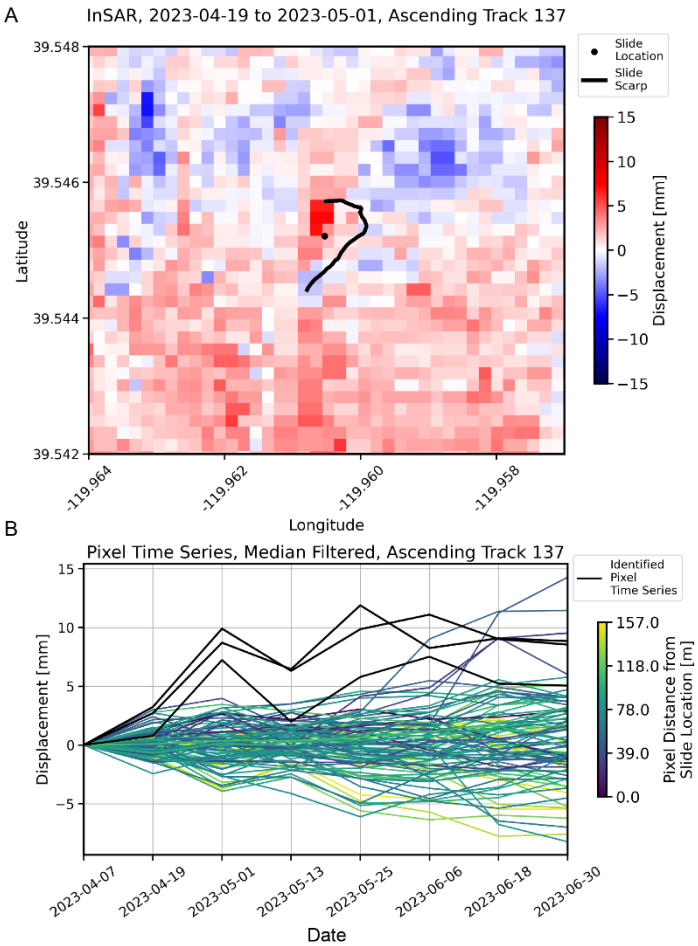

Figure 8. (A) InSAR map view of time series result between epochs of 04-19 to 05-01, 2023. Identified pixels are within the slide mass and stand out from surrounding pixels with regards to displacement (red pixels within the slide mass). InSAR image has not been de-ramped. (B) Time series plot of identified pixels (black) and nearby pixels colored by distance from center of the slide. Identified pixels are selected from figure 8A. The time series of these pixels (black, and correspond to the red pixels within the slide scarp in figure 8A) stand out compared to nearby pixels. Time series has been median filtered. Movement beyond median filtered neighbor time series is seen between 04-19 and 05-01, 2023.

WEATHER CONDITIONS (APRIL 26 TO MAY 1, 2023)

Weather conditions during the period from April 26 to May 1, 2023 were dry but featured the first heat wave of the season, which followed the aforementioned unusually cool, wet winter to early spring. Unusually heavy snowfall blanketed Peavine Mountain over the winter of 2023, such that trails and roads on the south flank of the mountain were still largely inaccessible by foot above elevations of ~6,000 ft (1,829 m) as late as mid-April. As shown in figure 9, temperatures ramped up rapidly in late April, with record highs of 86°F (30°C) recorded on both April 28 and 29 by the National Weather Service in Reno. A local weather station in the Somersett area recorded high temperatures of 80 to 82°F (27 to 28°C) on April 28, 29, and 30.

We suggest that these unseasonably warm conditions led to accelerated snowmelt and runoff from the upper slopes of Peavine Mountain, which in turn further saturated soils and ultimately triggered the landslide. The relatively high sun-angle in late April was probably an important factor in accelerating snowmelt on the south facing slopes of Peavine Mountain. Similar conditions in the spring of 1983 caused a major landslide off the south slopes of Slide Mountain in the Carson Range, which caused major damage and the loss of one life in Washoe Valley (Watters, 1983; Glancy and Bell, 2000). Spring heat waves following cool wet winters may be a primary recipe for triggering landslides in this region, particularly on snow laden, south-facing steep slopes.

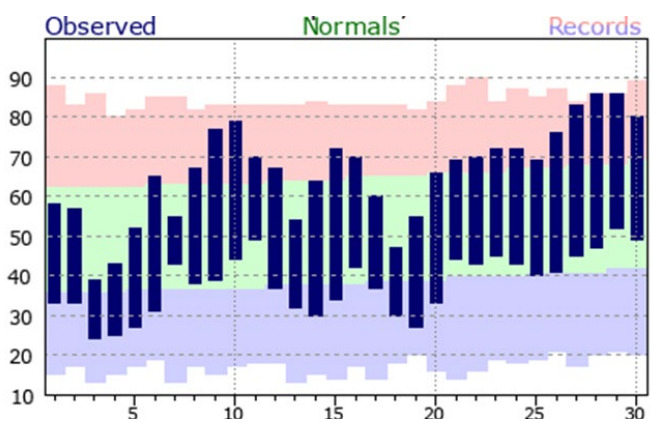

Figure 9. Chart of recorded temperatures for April 2023 for Reno, Nevada, from the National Weather Service. Note the record high temperatures on April 28 and 29. https://www.weather.gov/rev/CliPlot

DISCUSSION

As defined by Varnes (1978), landslides include a zone of depletion or extension, where the land surface is lowered, and a zone of accumulation, where earth materials either flow downslope or buckle or rise against adjacent topography (figure 10). Landslides commonly occur along preexisting discontinuities such as a bedding plane, a layer of weak material (weathered bedrock or saprolite), or the contact between colluvial materials and bedrock. The discontinuity is known as a slide plane and can be a curved (rotational slides), planar, or listric surface (translational slides) (figure 10). Rotational slides are typically associated with several back-tilted blocks at the head of the slide, whereas translational slides are associated with head scarp grabens. If the slide mass remains relatively intact, it is characterized as a block slide (Varnes, 1978).

Hungr et al. (2014) described several additional mechanisms for the occurrence of rock landslides including sliding on a surface of two planes with a downslope-oriented intersection (rock wedge slides), sliding on a surface of several planes of uneven curvature (rock compound slides), and sliding on an irregular surface consisting of randomly oriented joints/discontinuities (rock irregular slides). However, Hungr et al. (2014) also noted that because rock structure is not systematic (various discontinuities separated by segments of intact rock), rock landslides are commonly associated with complex mechanisms not easily characterized by a particular mechanism.

A wide variety of causal factors may influence the occurrence of landslides including natural erosion or deposition along slope margins, anthropogenic excavation or loading, and seismic activity, among others. However, the most common causes are related to weathering and water regime changes (p. 116, Fookes et al., 2007). Chemical, physical, and biological weathering of subsurface materials can result in changes in density, strength, and permeability, and lead to the development of weak discontinuities at depth. Ground water elevation changes and saturation of subsurface materials related to intense/long-duration rainfall, sustained snow melt, and flooding can lead to excess pore water pressure and changes in bulk density. In particular, the addition of water to clay-bearing materials decreases cohesion and the angle of internal friction, leading to a decrease in shear strength.

The 2023 landslide was associated with a distinct zone of extension along the head scarp and buckling at the toe of the slide. The landslide transported bedrock and the overlying colluvium as a block with limited internal deformation. The thrust scarps along the toe of the landslide and slickenlines in the deformed colluvium indicate that the slide mass transported the largely bedrock block toward the west-southwest resulting in thrust deformation of the

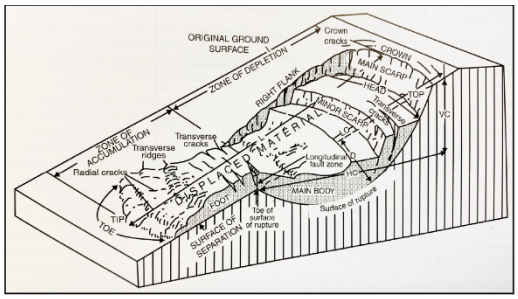

Fookes et al. (2007)

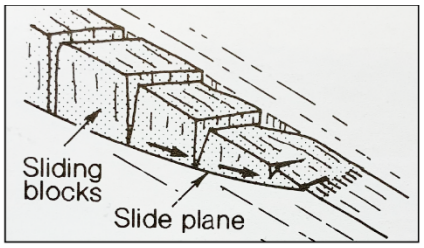

Ellen and Wieczorek (1998)

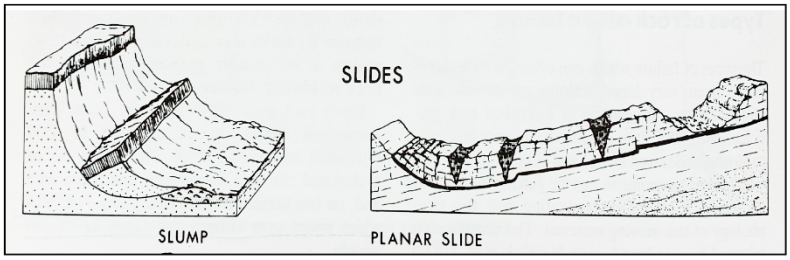

Selby (1993)

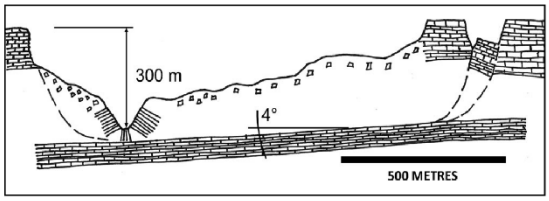

Varnes (1978)

Hungr et al. (2014)

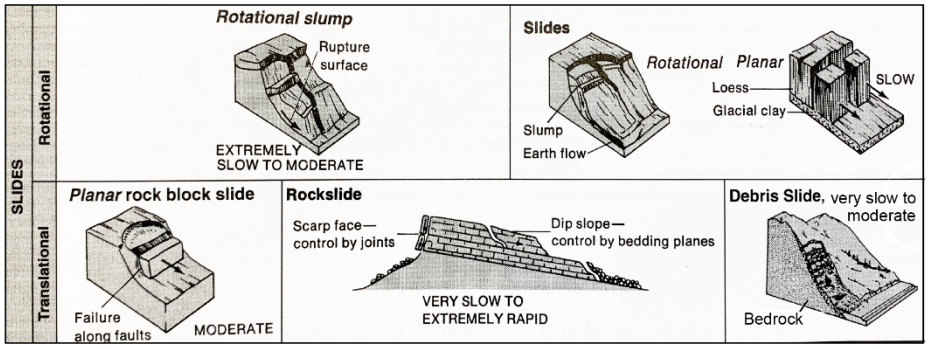

Figure 10. Schematic diagrams and terminology associated with rotational and translational landslides. Modified from Hungr et al. (2014), Ellen and Wieczorek (1988), Varnes (1978), Fookes et al. (2007), Selby (1993).

colluvium along the western bank of the drainage. Because the toe of the landslide consists primarily of bedrock, it did not appreciably break up and did not flow down the valley (no material flow downslope). The landslide mobilized along a slide plane of unknown geometry. Thus, based on the geomorphology of the head scarp (normal separation, extension, and graben formation), transverse cracks within the slide mass, and thrusting along the toe, the slide is best characterized as a translational block slide/slump or possibly a rock irregular slide. However, without subsurface data a rotational slide plane (rotational slide), wedge slide, or compound slide cannot be precluded.

The extreme winter of 2023 produced over 200% of the average annual precipitation for the Reno area. This precipitation (rain and snow) contributed to saturation of the colluvial sediments deposited across the hillslopes along the southern slopes of Peavine Mountain and likely increased local pore water pressure in the subsurface. The late April heat wave accelerated snowmelt, particularly on the south-facing slopes of the mountain, and further saturated colluvial sediments and soils in the area. The 2023 landslide was likely triggered by these climatic conditions. Additional contributing factors may include the thick colluvial deposits near the head scarp (loading), clay weathering of the bedrock and associated discontinuities, and possibly undercutting by the stream channel.

SUMMARY AND RECOMMENDATIONS

Our reconnaissance geologic and geomorphic evaluation has determined that the weathered andesite bedrock, locally thick clay-rich colluvium, and steep slopes along the south side of Peavine Mountain are susceptible to slope failures including rotational landslide slumps, planar slides, and debris flows. South-facing slopes in the region may be particularly vulnerable in spring heat waves following wet cool winters. Given the landslide hazard and existing/planned residential development in the area, NBMG recommends that future development efforts implement slope stability studies including mapping and geotechnical studies to better understand the landslide risk. These studies could include drilling to characterize subsurface materials (colluvial cover thickness, bedrock weathering, potential slide planes) and the installation of monitoring and instrumentation equipment (piezometers, extensometers, and tiltmeters). It is also recommended that a geotechnical engineer estimate a "Factor of Safety" for slopes adjacent to new developments. Any development in the immediate vicinity of the 2023 landslide should also include an assessment of additional motion. The photographs and measurements contained herein serve as baseline information for such an investigation.

CLOSURE AND LIMITATIONS

This report was prepared to convey the general characteristics of the 2023 landslide to the public. The observations and conclusions contained in this report are based on site conditions on the dates of the field reconnaissance discussed herein and represent the opinions of the authors. The information in this report should be considered preliminary and should not be used to determine areas of potential future slope instabilities. A significant amount of additional exploration and slope stability analysis is required to fully understand the cause of the 2023 landslide, as well as the potential for reactivation and/or expansion of the landslide.

ACKNOWLEDGMENTS

We thank the NBMG cartographic group for layout and formatting of this report. William Hammond provided review of the InSAR analysis.

REFERENCES

Digital Aerial Solutions, 2018, Lidar project report—NV Reno Carson City Urban: Prepared for U.S. Geological Survey, contract #16PC00044, task order #G17PD01257.

Ellen, S.D., and Wieczorek, G.F. (editors), 1988, Landslides, floods, and marine effects of the storm of January 3–5, 1982, in the San Francisco Bay region, California: U.S. Geological Survey Professional Paper 1434, 310 p.

Faulds, J.E., Koehler, R.D., and Henry, C.D., in review, Preliminary geologic map of the Verdi quadrangle, Washoe County, Nevada: Nevada Bureau of Mines and Geology Open-File Report 2023-XX, scale 1:24,000, X p.

Fookes, P.G., Lee, E.M., and Griffiths, J.S., 2007, Engineering Geomorphology, Theory and Practice: Whittles Publishing, CRC Press LLC, Scotland, UK.

Glancy, P.A., and Bell, J.W., 2000, Landslide induced flooding at Ophir Creek, Washoe County, western Nevada, May 30, 1983: U.S. Geological Survey Professional Paper 1617, 94 p.

Hungr, O., Leroueil, S., and Picarelli, L., 2014, The Varnes classification of landslide types, an update: Landslides, v. 11, p. 167–194.

National Oceanic and Atmospheric Administration (NOAA), 2023, California Nevada River Forecast Center, https://www.cnrfc.noaa.gov/monthly_precip.php. Accessed September 7, 2023.

Selby, M.J., 1993, Hillslope materials and processes, Oxford University Press Inc., New York, USA, second edition, 480 p.

Varnes, D.J., 1978, Slope movement types and processes, *in* Schuster, R.L., and Krizek, R.J., editors., Landslides—analysis and control: Transportation Research Board, National Research Council, Special report 176. National Academy of Sciences, Washington, D.C., pp. 12–33.

Watters, R.J., 1983, A landslide induced waterflood-debris flow: Bulletin of the International Association of Engineering Geology, no. 28, p. 177–182.

APPENDIX A

Photographs from observation site locations. See table 1 for more detailed descriptions of each site. Site #1 is along the access road north of the slide and not included here.

Site 2. View to south showing landslide head scarp (middle ground). Truckee River extends west to east in the lowlands. Carson Range in the background.

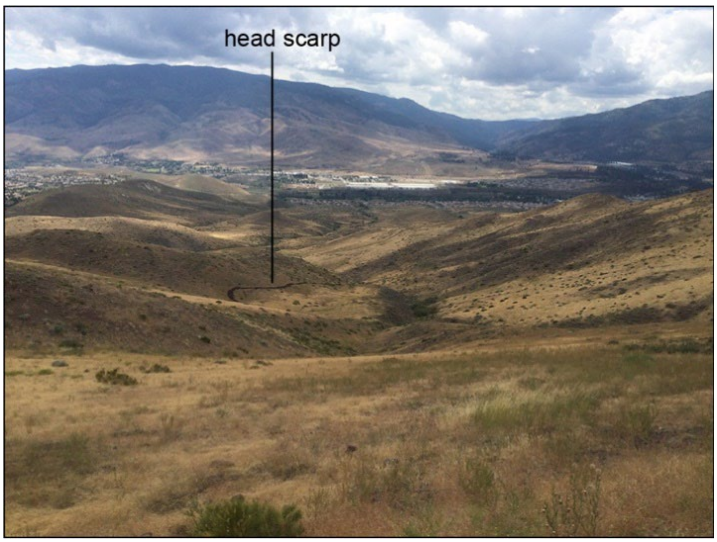

Site 3. View to the east of landslide head scarp and slide mass.

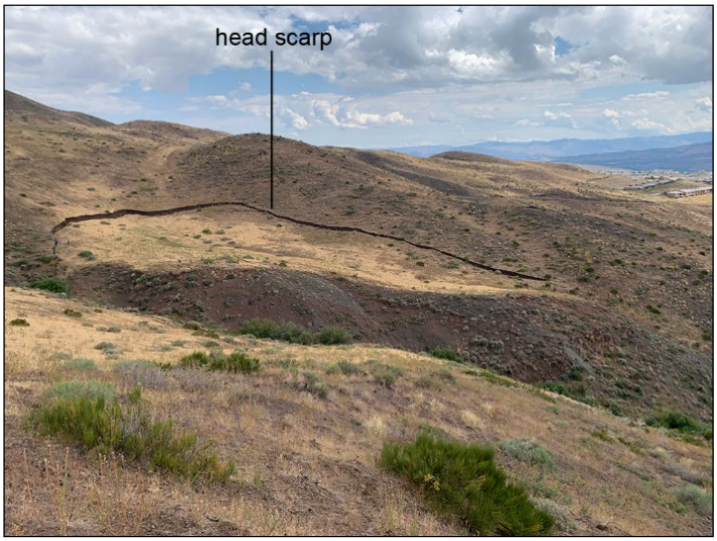

Site 4. View to the northeast of uphill-facing scarps along the lower western stream bank (left). Close-up view of uphill-facing scarp showing clay smear along slide plane (right).

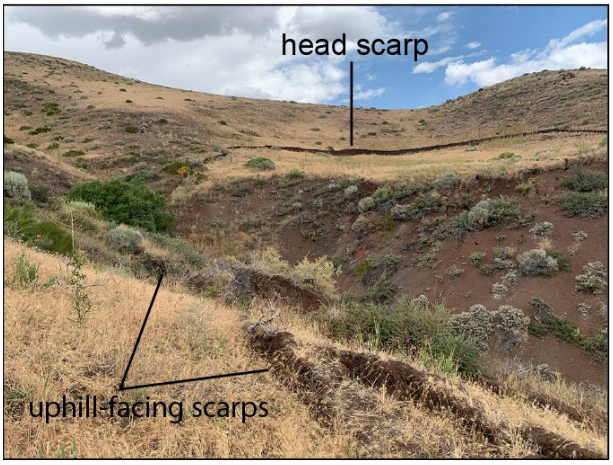

Site 5. View to the southeast (left) and north (right) along uphill-facing scarps along the west stream bank at the toe of the landslide.

Site 6. View southeast of extensional cracks and transverse ridges along the southern margin of the landslide toe.

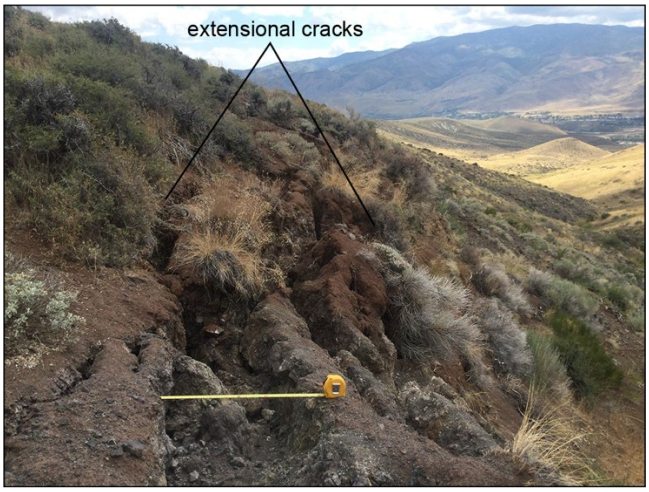

Site 6a. View to the northeast of the southern margin of the landslide head scarp (left) and southeast view of colluvial sediments exposed in the head scarp (right).

Site 7. View to the southwest of the head scarp and extensional graben along the southeastern margin of the landslide.

Site 8. View to the northeast of the head scarp along the southeastern margin of the landslide.

Site 9. Head scarp and graben along the easternmost part of the landslide (left) and extensional transverse cracks west of the head scarp (right).

Site 10. View to the northwest of graben and head scarp along the northern margin of the landslide (left), and view north of colluvial sediments exposed in the head scarp (right).

Site 11. View to the west of extensional graben and head scarp along the northwestern part of the landslide.

Site 12. Extensional cracks along the west-central part of the slide mass. View to the south (left), and view to the west (right).

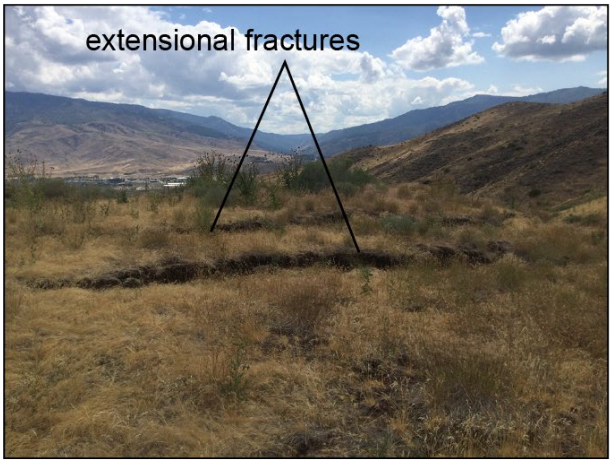

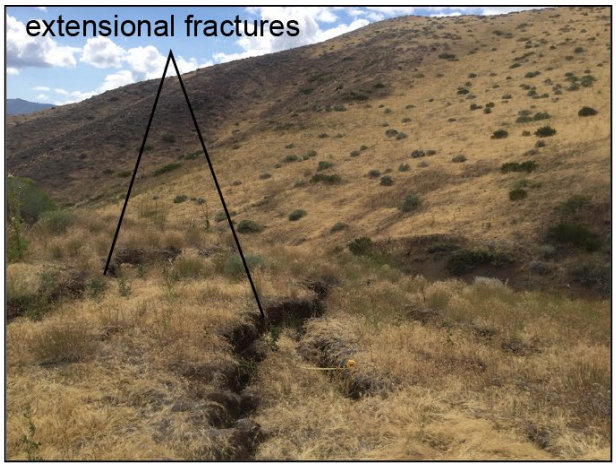

Nevada Bureau of Mines and Geology

nbmg.unr.edu

University of Nevada, Reno